J. Fluid Mech. (1983), *vol.* 129, *pp.* 455–471
Printed in Great Britain

Scale effects in a wave-refraction experiment

By TUDOR SPRINKS
Department of Mathematics, University of Essex

AND RONALD SMITH
Department of Applied Mathematics and Theoretical Physics, University of Cambridge

(Received 3 June 1982)

The experimental results of Provis (1975, 1976) for wave amplification at a conical island bear little resemblance to the theoretical predictions of Smith & Sprinks (1975). Here Provis's suggestion is confirmed: that his experiments were dominated by viscous damping and by standing waves between the island and the wavemaker. Estimates are given as to how large an experiment needs to be to avoid these important scale effects.

1. Introduction

Provis (1975, 1976) describes a series of experiments concerned with the possibility that waves can be trapped near a conical island by the effects of refraction. These experiments were originally designed to test the resonance-frequency predictions of Shen, Meyer & Keller (1968). More recently Smith & Sprinks (1975) have calculated the wave-amplitude response for the scattering at a conical island of a plane wave incident from infinity. Neither the resonance frequencies nor the amplitude predictions were borne out by the experiments.

The wave basin used by Provis (1975, 1976) was 5.55 m wide and 5.80 m long, and occupied almost the whole area of a small 4th-floor laboratory. For structural reasons the water depth, in consideration of the floor loading, was limited to 0.15 m. The waves were generated by a plane movable flap 3.75 m long, which was hinged at the basin floor. Plane beaches were placed on the other three sides of the basin to absorb waves – both the progressive waves and those scattered by the topography. Most of Provis's experiments involved in a cone of radius 1.5 m with a slope of 1 : 10. The water level in the tank was adjusted so that the vertex of the cone formed an island of the required radius (see figure 1). The area of the basin was such that keeping the surface clean posed some problems. When measurements were not being made the surface was continually being skimmed by having a slow flow of water into the basin and allowing the excess to flow over a weir.

It is natural to attribute the failure of the theoretical predictions to scale effects in the laboratory-sized experiments. Provis (1975) gives theoretical and experimental evidence to suggest that viscous damping and wave interactions between the island and the wavemaker were of particular importance. Here we take up Provis's suggestion and we give the appropriate modifications of the wave-amplitude predictions. A useful by-product is an estimate as to how large an experiment would have to be to simulate correctly oceanic conditions of effectively undamped waves in an effectively infinite ocean.

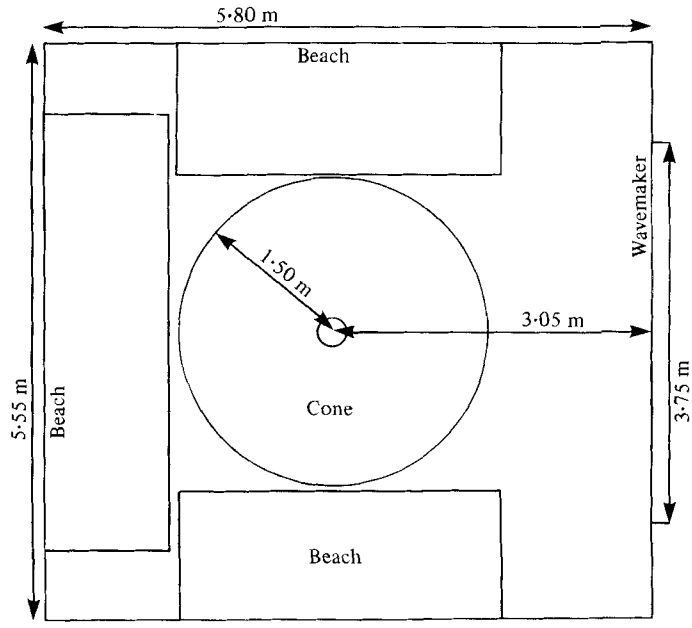

FIGURE 1. Plan of Provis's (1975) experiment.

2. Viscous damping

In a related experiment, involving a submerged circular sill, Pite (1977) found a similar disparity with the theoretical predictions of Longuet-Higgins (1967). However, Pite managed to suppress the standing waves and hence to isolate the effects of viscous damping. He showed that to account for the considerable reduction in amplification it sufficed that in each region of constant depth the local wavenumber be determined as the complex solution of the viscous dispersion relation.

For water with an inextensible surface film and with surface tension ignored, the calculation procedure given by Lamb (1932, §349) leads to the dispersion relation (see appendix)

$$\omega^2\left\{1-\frac{k\tanh kh}{m\tanh mh}\right\}=gk\tanh kh\left\{1-\frac{2k\coth kh}{m\tanh mh}+\left(\frac{k}{m}\right)^2+\frac{2k\,\mathrm{cosech}\,kh}{m\sinh mh}\right\}, \quad (2.1a)$$

with

$$m^2=\mathrm{i}\omega/\nu+k^2, \quad (2.1b)$$

where ω is the wave frequency, k the complex wavenumber, h the water depth and ν the viscosity. If k_0 denotes the wavenumber in the absence of viscosity, then for small viscosity the leading-order correction is given by

$$k'=\left(\frac{\nu}{\mathrm{i}\omega}\right)^{\frac{1}{2}}\frac{\coth k_0h-\frac{1}{2}\tanh k_0h}{c_p c_g}, \quad (2.2)$$

where c_p, c_g are the local phase and group velocities.

In gently shoaling water the effects of viscosity can be expected to be locally almost the same as for water of constant depth. An appropriate modification to the mild-

slope equation (Berkhoff 1973; Jonsson & Brink-Kjaer 1973; Smith & Sprinks 1975) is

$$\nabla\cdot((c_{\mathrm{p}}c_{\mathrm{g}}-\delta_1+\mathrm{i}\delta_2)\nabla\zeta)+\omega^2\left(\frac{c_{\mathrm{g}}}{c_{\mathrm{p}}}\right)\zeta=0, \tag{2.3a}$$

$$\delta_1=\delta_2=\left(\frac{\nu}{2\omega}\right)^{\frac{1}{2}}g(1+\operatorname{sech}^2 k_0 h). \tag{2.3b}$$

For clean water (with no appreciable surface film or scum) there is only significant viscous damping at the rigid bed and only the $\operatorname{sech}^2 k_0 h$ part of the factor in (2.3*b*) need be retained. Since viscosity is primarily of importance in shallow water (owing to the reduced wavelength and increased amplitude), and where $\operatorname{sech}^2 k_0 h = 1$, to a good approximation the clean-water results correspond to a quartering of the viscosity.

We remark that it is the structure of the thin viscous Stokes' layers near the free surface and the rigid bed that makes it appropriate to model the viscous corrections as second derivatives rather than as lower-order terms. For example, the lower boundary condition for the inviscid flow in the interior of the fluid is

$$\frac{\partial\phi}{\partial z}+\nabla h\cdot\nabla\phi=\left(\frac{\nu}{\mathrm{i}\omega}\right)^{\frac{1}{2}}\nabla^2\phi \quad (z=-h) \tag{2.4}$$

(Mahony 1971, §5), where ϕ is the velocity potential and ∇ the horizontal derivative operator $(\partial_x, \partial_y, 0)$. As shown by Smith & Sprinks (1975, appendix A), the mild-slope equation can be derived formally by taking the $\cosh[k_0(z+h)]/\cosh k_0 h$ vertical component of the full three-dimensional linear water-wave equations. At the channel bed the velocity potential is reduced by a factor $\operatorname{sech} k_0 h$. Another factor of $\operatorname{sech} k_0 h$ arises in taking the weighted vertical average of the full equations. Thus the viscous correction term in (2.4) yields the $\operatorname{sech}^2 k_0 h$ term in a formal derivation of (2.3*a*, *b*). Likewise, the modification associated with the inextensible surface film (if present) can be derived from the upper boundary condition

$$\partial_z\phi-\frac{\omega^2\phi}{g}=-\left(\frac{\nu}{\mathrm{i}\omega}\right)^{\frac{1}{2}}\phi \quad (z=0). \tag{2.5}$$

3. Scattering of damped waves

The scattering theory given by Smith & Sprinks (1975, §4) for circularly symmetric islands has to be changed in several minor respects. First, the far-field wavenumber κ for waves coming in from the right now has a negative imaginary part

$$\kappa^2(c_{\mathrm{p}}c_{\mathrm{g}}-\delta_1+\mathrm{i}\delta_2)_\infty=\omega^2\left(\frac{c_{\mathrm{g}}}{c_{\mathrm{p}}}\right)_\infty. \tag{3.1}$$

This means that the waves must have been generated at a finite distance from the island. For this same reason the complex amplification factors A_m in the Fourier-series representation of the waves

$$\zeta=A_0\zeta_0(r)+2\sum_{m=1}^{\infty}A_m\zeta_m(r)\cos m\theta \tag{3.2}$$

depend on our choice of the reference position. So for mathematical convenience we take the reference wave height to be that of the incident wave along the y-axis (i.e. the incident wave before it reaches the island is written $\mathrm{e}^{\mathrm{i}\kappa x}$).

Secondly, at a beach the attenuation terms δ_1, δ_2 give rise to a singular perturbation in so far as they move the singular point slightly in the ordinary differential equation for $\zeta_m(r)$:

$$\frac{\mathrm{d}}{\mathrm{d}r}\left((c_\mathrm{p}c_\mathrm{g}-\delta_1+\mathrm{i}\delta_2)\,r\frac{\mathrm{d}\zeta_m}{\mathrm{d}r}\right)+\left(\omega^2\frac{c_\mathrm{g}r}{c_\mathrm{p}}-\frac{m^2}{r}(c_\mathrm{p}c_\mathrm{g}-\delta_1+\mathrm{i}\delta_2)\right)\zeta=0, \tag{3.3a}$$

with

$$\zeta_m=1 \quad (r=a). \tag{3.3b}$$

In the derivation of (2.2, 2.3) it is implicit that locally the effect of the viscous term is small. Thus for consistency we must choose the boundary conditions for ζ_m such that near the shoreline $r=a$ the solution is not a singular perturbation (i.e. the shoreline motion is forced by the incident waves and not vice versa). To do this we represent ζ_m explicitly as a regular perturbation expansion with respect to both $\rho=(r-a)/a$ and $(\nu/2\omega a^2\alpha^2)^{\frac{1}{2}}$:

$$\zeta_m=1-\rho\left\{\frac{\omega^2 a}{\alpha g}+(1-\mathrm{i})\left(\frac{\nu}{2\omega a^2\alpha^2}\right)^{\frac{1}{2}}\left[m^2+\frac{\omega^2 a}{\alpha g}-\left(\frac{\omega^2 a}{\alpha g}\right)^2\right]\right\}+\ldots, \tag{3.4}$$

where α is the beach slope (cf. Smith & Sprinks 1975, appendix B). In practice it has been found that the same results are achieved simply by using a computational stepsize much *larger* than the region in which the δ-terms dominate. Presumably this is the case because in a finite-difference scheme it is implicit that a power-series representation can be used.

Thirdly, the radiation condition must be replaced by the seemingly different requirement that the scattered wave $\zeta-\mathrm{e}^{\mathrm{i}\kappa x}$ decays exponentially away from the island. Thus, any exponentially growing terms in ζ must be exactly cancelled by corresponding terms in $\mathrm{e}^{\mathrm{i}\kappa x}$. This leads to the condition

$$A_m\,\zeta_m(r)\sim\tfrac{1}{2}\mathrm{i}^m H_m^{(1)}(\kappa r) \quad \text{as} \quad r\to\infty. \tag{3.5}$$

Since ζ_m can only be determined numerically and may have systematic errors, (3.5) itself is not an accurate basis for evaluating A_m. However, the integral formulation of (3.3a) which is presented by Smith & Sprinks (1975) provides us with the more robust relationship

$$\zeta_m=L_m J_m(\kappa r)-M_m\,Y_m(\kappa r) \quad (r>b), \tag{3.6}$$

where b is the radius of the island shelf. The complex linear functional L_m is defined by

$$L[\zeta_m]=\frac{\pi}{2}a\frac{\bar{p}(a)}{\bar{p}_\infty}\left(\zeta_m\kappa Y_m'(\kappa a)-Y_m(\kappa a)\frac{\mathrm{d}\zeta_m}{\mathrm{d}r}\right)_{r=a}$$
$$+\frac{\pi}{2}\int_a^b\zeta_m(r)\left\{\frac{\kappa}{\bar{p}_\infty}\frac{\mathrm{d}\bar{p}}{\mathrm{d}r}\,Y_m'+\frac{\omega^2(q\bar{p}_\infty-\bar{p}q_\infty)\,Y_m}{\bar{p}_\infty^2}\right\}r\,\mathrm{d}r, \tag{3.7a}$$

with

$$\bar{p}=c_\mathrm{p}c_\mathrm{g}-\delta_1+\mathrm{i}\delta_2, \quad q=\frac{c_\mathrm{g}}{c_\mathrm{p}} \tag{3.7b}$$

and for M_m we simply replace Y_m by J_m. The integrand in (3.7a) decays away from the shoreline and thereby annuls any systematic numerical errors in ζ_m, particularly at high frequencies. Using the relationship (3.6) in (3.5) we have

$$|A_m|=|L_m+M_m|^{-1}, \quad \arg(A_m)=\tfrac{1}{2}m\pi-\arg(L_m+\mathrm{i}M_m). \tag{3.8}$$

Figure 2(a) shows the results obtained by Smith & Sprinks (1975, figure 5) for the conical island geometry

$$h=0.1(r-a) \quad (a<r<20a). \tag{3.9}$$

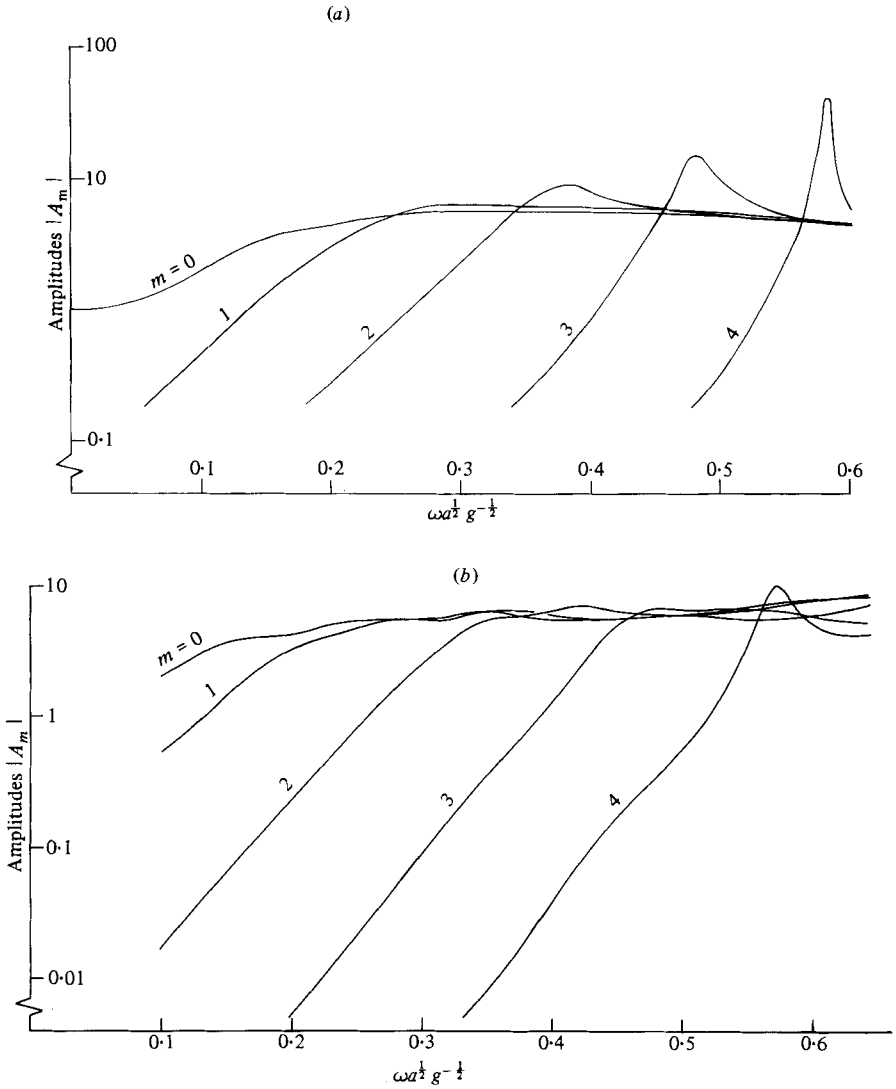

FIGURE 2. Frequency dependence of the shoreline amplitude factors $|A_m|$ for a conical island in an infinite basin: (*a*) with viscosity neglected; (*b*) with viscosity included.

Figure 2 (*b*) shows the corresponding results when there is an inextensible surface film and with the non-dimensional viscosity appropriate to Provis' (1975) experiments

$$\nu g^{-\frac{1}{2}} a^{-\frac{3}{2}} = 2 \times 10^{-5}. \tag{3.10}$$

In accord with physical intuition and with the results of Pite (1977) for the circular sill, we see that the main effects of damping are to widen the resonance humps and to reduce the wave amplitudes, particularly at high frequencies.

4. Standing waves between a wavemaker and an island

In a qualitative attempt to explain the occurrence of standing waves in Provis's (1975) experiments, Smith (1975) has pointed out the existence of virtual trapped standing-wave modes. These modes correspond to rays that repeatedly reflect back

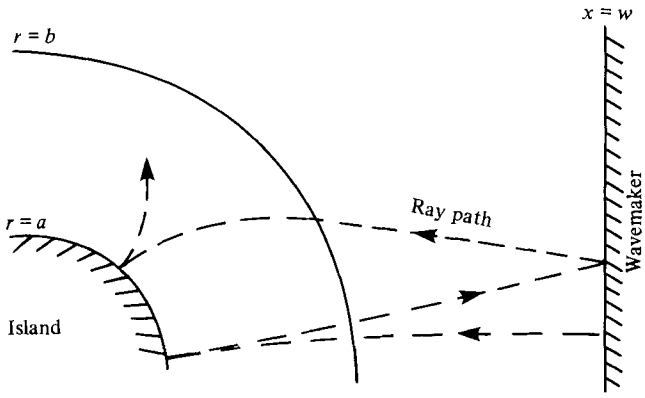

FIGURE 3. Ray paths for the reflection of wave energy between the wavemaker and the island.

and forth between the wavemaker and the island (see figure 3). In accord with this ray description, Smith's resonance-frequency predictions correspond to there being a large integer number of half-wavelengths between the wavemaker and the island, i.e.

$$\omega\left\{\int_a^b \frac{\mathrm{d}r}{c_\mathrm{p}}+\frac{w-b}{(c_\mathrm{p})_\infty}\right\} = (n+\tfrac{1}{4})\,\pi. \tag{4.1}$$

Here w is the distance from the centre of the island to the wavemaker, and the extra factor $\frac{1}{4}\pi$ comes from the Bessel-function form of the waves close to the shoreline (Shen & Keller 1975). The analysis of this section can be regarded as being the quantitative counterpart of the previous work of Smith (1975).

Our aim is to solve (2.3a) subject to the wavemaker boundary condition

$$\frac{\partial\zeta}{\partial x} = \mathrm{i}\kappa\,\mathrm{e}^{\mathrm{i}\kappa x} \quad (x = w), \tag{4.2}$$

and to the far-field condition that the scattered wave $\zeta-\mathrm{e}^{\mathrm{i}\kappa x}$ is outgoing. The normalization of the wavemaker motion has been chosen to ensure that as w tends to infinity the solution for ζ tends to that of the idealized case of a wave incident from infinity.

Over the island shelf we again use the Fourier-series representation

$$\zeta = \sum_{m=-\infty}^{\infty} A_m\,\zeta_m(r)\cos m\theta, \quad \text{with} \quad A_{-m} = A_m, \quad \zeta_{-m} = \zeta_m. \tag{4.3}$$

However, in the constant-depth outer region $r > b$ a more appropriate representation is

$$\zeta = \mathrm{e}^{\mathrm{i}\kappa x} + \sum_{m=-\infty}^{\infty} \mathrm{i}^m B_m\{H_m^{(2)}(\kappa r)\cos m\theta + H_m^{(2)}(\kappa\hat{r})\cos m\hat{\theta}\}, \tag{4.4}$$

where $B_{-m} = B_m$ and $\hat{r}$, $\hat{\theta}$ are the polar coordinates with respect to the image island (see figure 4). The conjunction of real and image island terms ensures that both the wavemaker and far-field conditions are satisfied.

Sufficiently close to the edge of the island shelf (i.e. $b < r < 2w$) we can use Graf's formula (Abramowitz & Stegun 1964, equation (9.1.79)) together with the Bessel-function representation for $\mathrm{e}^{\mathrm{i}\kappa x}$ to get

$$\zeta = \sum_{m=-\infty}^{\infty}\left[\mathrm{i}^m + \mathrm{i}^m B_m + \sum_{l=-\infty}^{\infty} \mathrm{i}^l H_{m+l}^{(2)}(2\kappa w)\,B_l\right] J_m(\kappa r)\cos m\theta$$
$$-\mathrm{i}\sum_{m=-\infty}^{\infty} \mathrm{i}^m B_m\,Y_m(\kappa r)\cos m\theta. \tag{4.5}$$

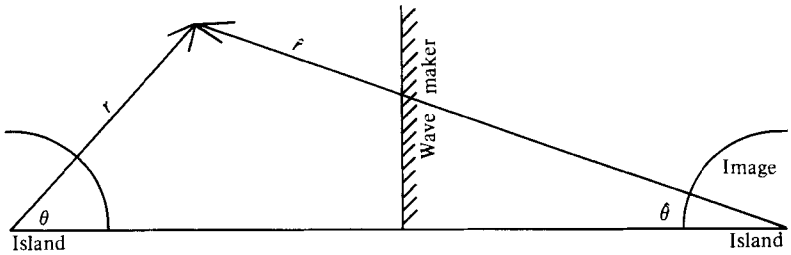

FIGURE 4. Definition sketch of the polar coordinates (r, θ) and $(\hat{r}, \hat{\theta})$ relative to the real and image islands.

Alternatively, using the relationship (3.6) we have

$$\zeta = \sum_{m=-\infty}^{\infty} A_m L_m J_m(\kappa r) \cos m\theta - \sum_{m=-\infty}^{\infty} A_m M_m Y_m(\kappa r) \cos m\theta. \tag{4.6}$$

Equating like terms in the two Bessel-function representations (4.5), (4.6), we can derive coupled linear equations involving only the A_m coefficients:

$$A_m(L_m + \mathrm{i}M_m) + \mathrm{i} \sum_{l=-\infty}^{\infty} M_l H_{m+l}^{(2)}(2\kappa w) A_l = \mathrm{i}^m \quad (-\infty < m < \infty). \tag{4.7}$$

A less elegant but numerically more convenient formulation is

$$A_m(L_m + \mathrm{i}M_m) + \mathrm{i}A_0 M_0 H_m^{(2)} + \mathrm{i} \sum_{l=1}^{\infty} A_l M_l (H_{m+l}^{(2)} + (-1)^{\min(l,m)} H_{|m-l|}^{(2)}) = \mathrm{i}^m \quad (m \geqslant 0), \tag{4.8}$$

where the argument $2\kappa w$ of the Hankel functions has been suppressed.

For Provis's (1975) experiments the wavemaker was situated at about forty island radii from the centre of the conical island. Figures 5(*a–e*) show the undamped predictions of the amplitude factors $|A_m|$ for this particular geometry. As an aid to interpretation the figures show the standing-wave resonance predictions ($n = 5, \ldots, 9$) derived from (4.1), and the edge-wave resonance predictions ($m = 1, \ldots, 4$) derived from the work of Smith (1974). Weak resonances ean be identified close to each of these frequencies. Moreover, the responses are not restricted to a single Fourier component A_m. By contrast with figures 2(*a, b*), the proximity of the wavemaker makes the results complicated, and qualitatively very similar to Provis's (1975) figures (6.3)–(6.5). Thus we confirm Provis's assessment that his experiments were dominated by the effects of standing waves between the wavemaker and the island.

5. Amplitude and phase maps

For tsunamis it is the wave height at the shoreline which is of primary interest. Hence the emphasis upon the complex amplification factors A_m (we recall that the radial functions $\zeta_m(r)$ are normalized to be equal to 1 at the shoreline). However, there is a wealth of additional information in the rest of the wave-field (Berkhoff 1976; Jonsson & Skovgaard 1979).

Having separately analysed the effects of viscous damping and of island–wavemaker interactions, it is straightforward to allow simultaneously for both effects (i.e. to allow κ to be complex in (4.8)). Figure 6(*a–c*) gives amplitudes and phase predictions close to the island at the frequencies

$$\omega a^{\frac{1}{2}} g^{-\frac{1}{2}} = 0.3,\ 0.45,\ 0.6, \tag{5.1}$$

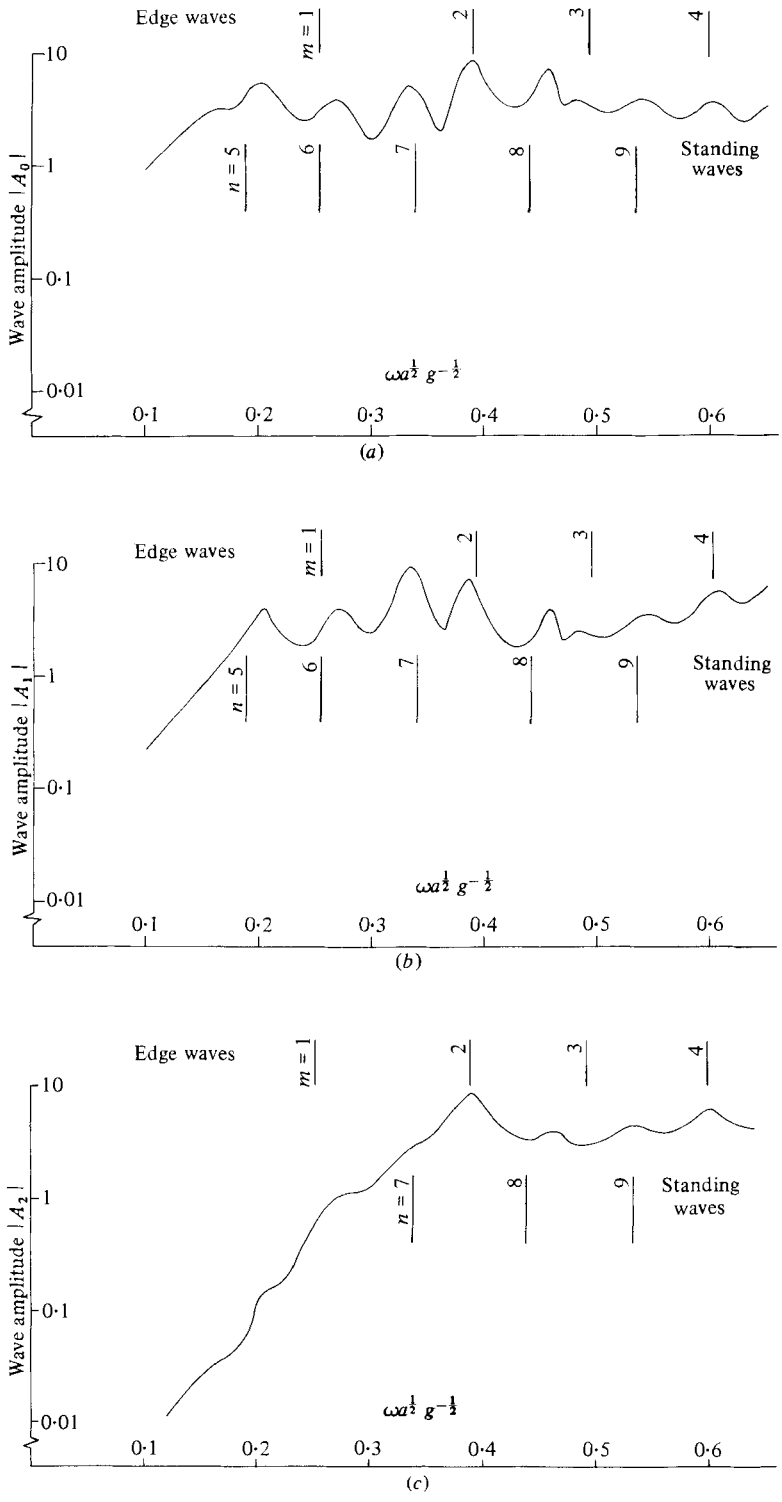

FIGURE 5(*a–c*). For caption see facing page.

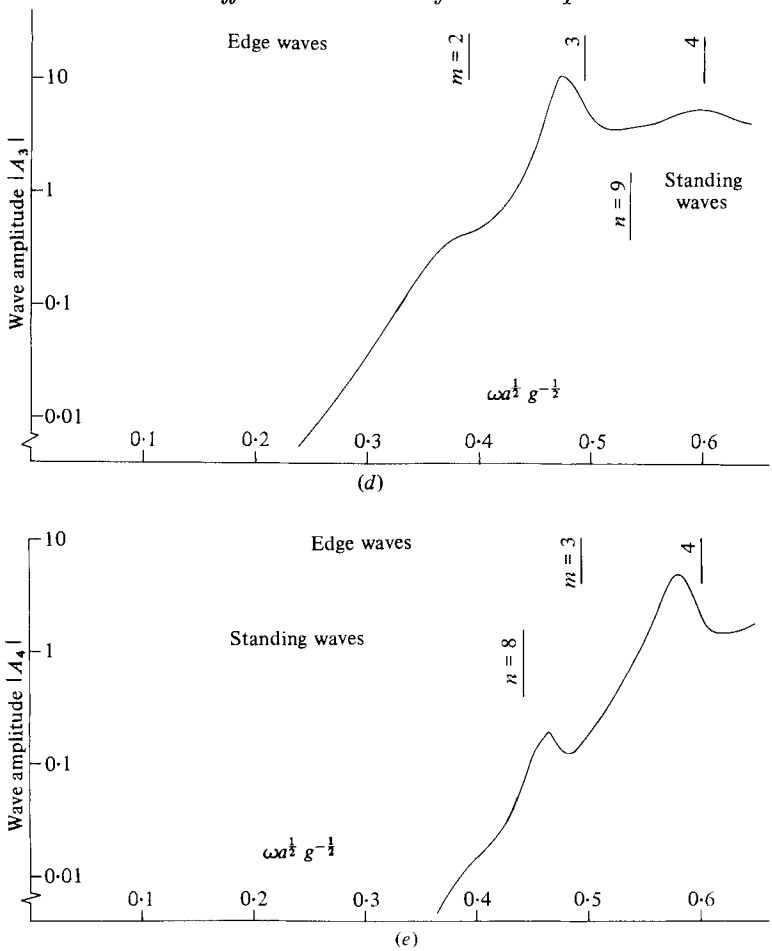

FIGURE 5. Frequency dependence of the shoreline amplitude factors (*a*) $|A_0|$, (*b*) $|A_1|$, (*c*) $|A_2|$, (*d*) $|A_3|$, (*e*) $|A_4|$ with no viscosity but with a wavemaker at distance $40a$ from the centre of the island.

when the non-dimensional viscosity has the value

$$\nu g^{-\frac{1}{2}} a^{-\frac{3}{2}} = 2 \times 10^{-5}, \tag{5.2}$$

and the water surface is assumed to be clean. In accord with the earlier results of figures 2 and 5 there is a progression from two to four amplification lobes near the shoreline as the higher Fourier components get excited. However, the dominant feature is simply the bending around and running-up of the incident waves at the front of the island.

Figure 7 shows the experimental results obtained by Provis (1975) for the case

$$\omega a^{\frac{1}{2}} g^{-\frac{1}{2}} = 0.462, \quad b = 21.3a, \quad w = 43.3a. \tag{5.3}$$

The resemblance to figure 6(*b*) is less than we might have hoped. However, Provis (1975) comments that when the phase measurements were made the possibility of amphidromic points was not considered, and there are probably additional amphidromic points which were not resolved. For the wave amplitudes there is no such ready excuse. Close to the island the observed wave amplitudes are smaller than predicted (possibly due to nonlinear and surface-tension effects at the water line). Also, behind the island there are not the distant regions with amplitude in excess of 2.

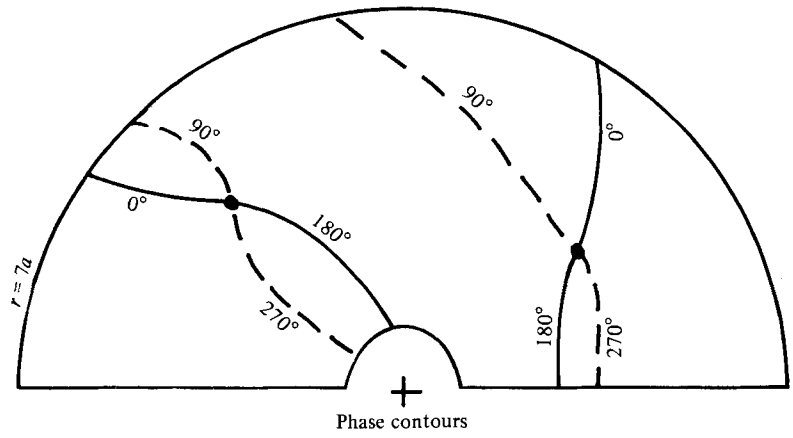

Phase contours

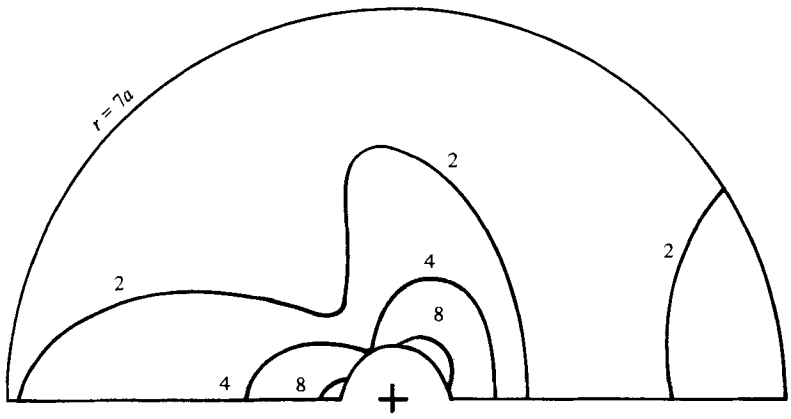

Amplitude contours (values 2, 4, 8)

(*a*)

FIGURE 6(*a*). For caption see p. 466.

The sensitivity of the results to the precise frequency, shelf radius, and wavemaker position, is insufficient to explain these errors. Presumably the fault lies in the many remaining deviations between idealization and experiment. For example, the slow drift of water in the experiments (the surface-skimming system) might not have swept away the surface scum close to the island, the three beaches in the experiment (see figure 1) cause additional damping, and the wavemaker was of limited extent (the effect of which is compounded by the refraction of wave energy towards the island). Rather than pursuing these more minor departures between theory and experiment, §6 asks instead how could the major difficulties, of viscosity and of standing waves, be avoided.

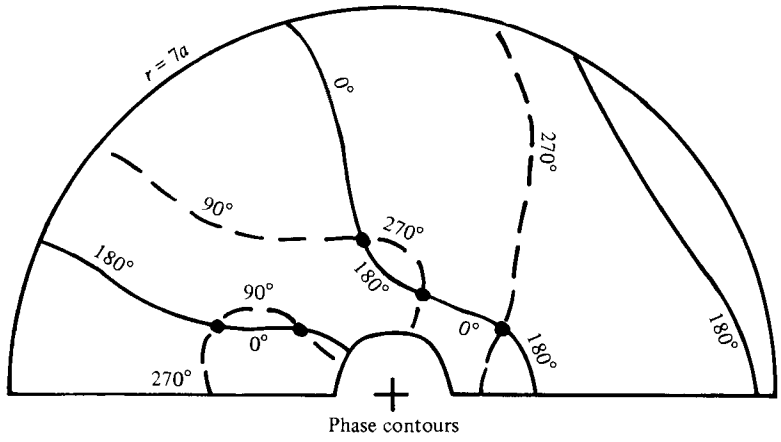

Phase contours

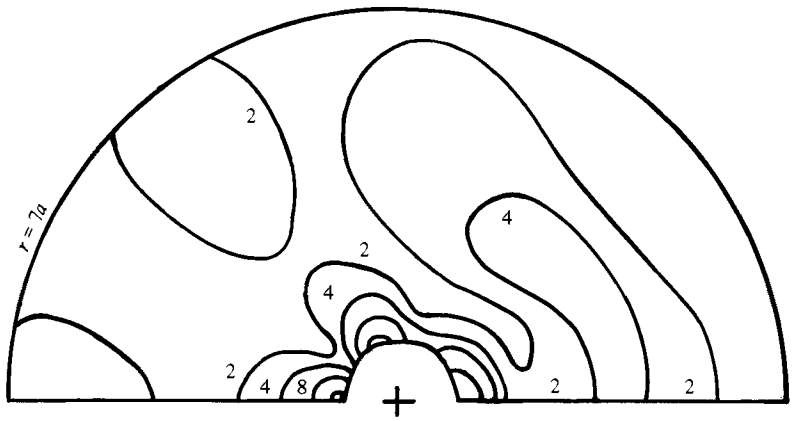

Amplitude contours (values 2, 4, 8, 16)

(*b*)

FIGURE 6(*b*). For caption see p. 466.

6. Avoiding scaling troubles

In assessing the effects of viscosity we can consider separately the far and near island effects. Across the island shelf we can use the deep-water attenuation rate to assess that there will *not* be significant fore–aft amplitude differences if

$$2b\,\mathrm{Im}\,(\kappa) \sim bk_\infty \left(\frac{\nu}{2\omega}\right)^{\frac{1}{2}} \frac{g}{(c_p c_g)_\infty} \tag{6.1}$$

is small. For the conditions of figure 6(*b*) this attenuation exponent has the value 0.02, and is indeed small.

To analyse the waves close to the island we follow Shen & Keller (1975) and pose the representation

$$\zeta_m = C(r)\frac{J_0(2[\xi(r)+\Delta]^{\frac{1}{2}})}{J_0(2\Delta^{\frac{1}{2}})} = C\psi(\xi), \tag{6.2a}$$

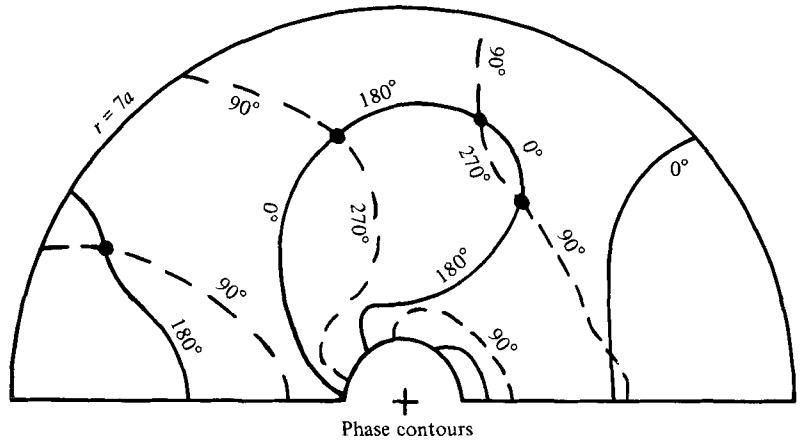

Phase contours

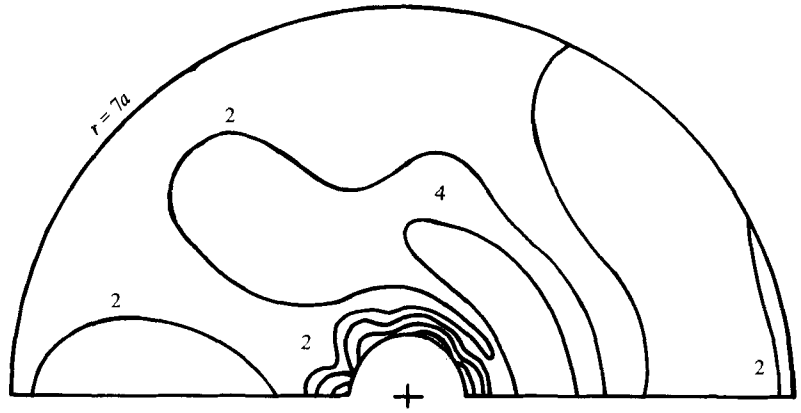

Amplitude contours (values 2, 4, 8, 16)

(c)

FIGURE 6. Contours of the predicted amplitude and phase (relative to the incident waves) near the conical island when the non-dimensional frequency $\omega a^{\frac{1}{2}} g^{-\frac{1}{2}}$ has the values (a) 0.3, (b) 0.45, (c) 0.6. Amphidromic points on the phase contours are indicated by the large dots.

where

$$\frac{\mathrm{d}}{\mathrm{d}\xi}\left([\xi+\Delta]\frac{\mathrm{d}\psi}{\mathrm{d}\xi}\right)+\psi=0, \tag{6.2b}$$

$$\xi=0, \quad C=1 \quad (r=a). \tag{6.2c}$$

Thus the comparison function ψ has the same structure near the beach as does the radial function $\zeta_m(r)$. This means that the amplitude and argument functions $C_m(r)$, $\xi_m(r)$ are slowly varying, at least in the vicinity of the beach.

Substituting the representation (6.2a) into the differential equation (3.3a) and separating out coefficients of ψ and of $[\xi+\Delta]\,\mathrm{d}\psi/\mathrm{d}\xi$, we derive the coupled equations

$$\frac{1}{\xi+\Delta}\left(\frac{\mathrm{d}\xi}{\mathrm{d}r}\right)^2=\frac{\omega^2 c_{\mathrm{g}}/c_{\mathrm{p}}}{c_{\mathrm{g}}c_{\mathrm{p}}-\delta_1+\mathrm{i}\delta_2}-\frac{m^2}{r}+\frac{1}{(c_{\mathrm{g}}c_{\mathrm{p}}-\delta_1+\mathrm{i}\delta_2)\,rC}\frac{\mathrm{d}}{\mathrm{d}r}\left((c_{\mathrm{g}}c_{\mathrm{p}}-\delta_1+\mathrm{i}\delta_2)\,r\frac{\mathrm{d}C}{\mathrm{d}r}\right), \tag{6.3a}$$

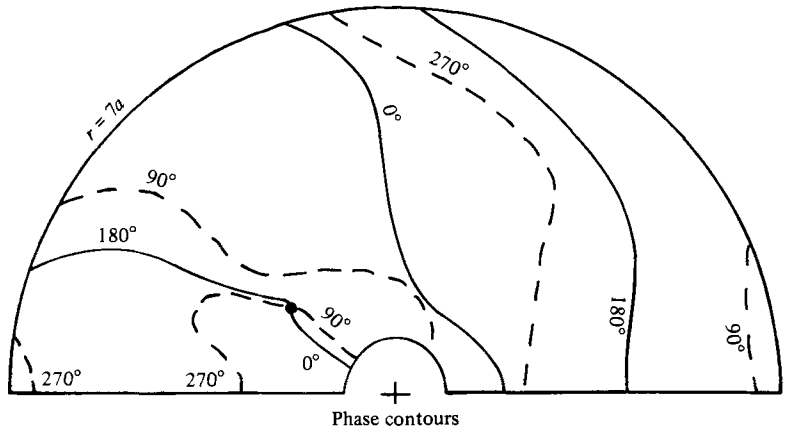

Phase contours

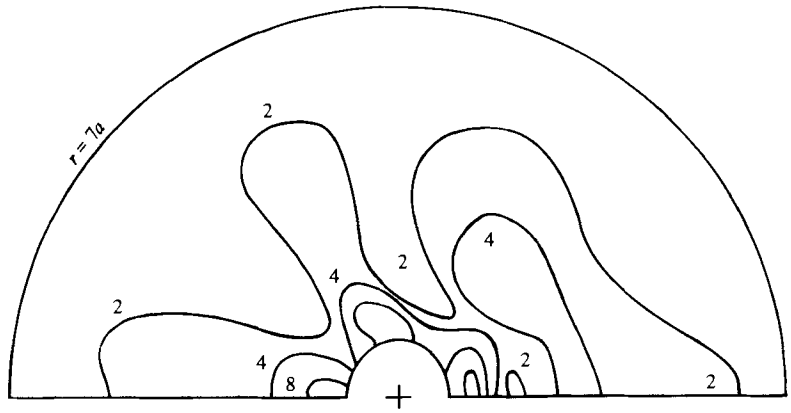

Amplitude contours (values 2, 4, 8, 16)

FIGURE 7. Provis's (1975) experimental results for the relative amplitude and phase of waves with frequency 5.449 rad s^{-1} near a conical island of slope 0.1, radius 70.5 mm and shelf radius 1.50 m, with a wavenumber at distance 3.05 m.

$$C^2 = \left[(-\delta_1 + \mathrm{i}\delta_2)\frac{\mathrm{d}\xi}{\mathrm{d}r}\right]_{r=a} \frac{a(\xi+\Delta)}{r\Delta(c_\mathrm{p}c_\mathrm{g} - \delta_1 + \mathrm{i}\delta_2)\,\mathrm{d}\xi/\mathrm{d}r}. \tag{6.3b}$$

If we neglect the derivatives of C, then the eikonal equation (6.3a) can be integrated:

$$2[\xi+\Delta]^{\frac{1}{2}} = 2\Delta^{\frac{1}{2}} + \int_a^r \left[\frac{\omega^2 c_\mathrm{g}/c_\mathrm{p}}{c_\mathrm{p}c_\mathrm{g} - \delta_1 + \mathrm{i}\delta_2} - \frac{m^2}{r^2}\right]^{\frac{1}{2}} \mathrm{d}r. \tag{6.4}$$

The displacement Δ of the singular position is chosen, as in (3.4), so that the effect of damping is a regular perturbation:

$$\Delta = \left(\frac{-\mathrm{i}\nu}{\omega a^2\alpha^2}\right)^{\frac{1}{2}} \frac{\omega^2 a}{\alpha g}, \quad \xi \sim \frac{\omega^2}{\alpha g}(r-a). \tag{6.5a,b}$$

In the representation (6.2a), the radial function ζ_m is diminished by a factor $J_0(2\Delta^{\frac{1}{2}})$.

Neumann's addition formula (Abramowitz & Stegun 1964, equation (9.1.75)) enables us to express Bessel functions of complex argument:

$$J_0(u+\mathrm{i}v) = J_0(u)\,I_0(v) + 2\sum_{k=1}^{\infty} J_k(u)\,I_k(v)\,\mathrm{i}^{-k}. \tag{6.6}$$

Thus for large Δ the viscous attenuation varies exponentially with $2\Delta^{\frac{1}{2}}$ (i.e. the modified Bessel functions I_k grow exponentially). Hence, the effect of damping close to the island will *not* be significant if

$$2\left(\frac{\nu}{\omega a^2\alpha^2}\right)^{\frac{1}{4}}\left(\frac{\omega^2 a}{\alpha g}\right)^{\frac{1}{2}} = 2\left(\frac{\nu\omega^3}{\alpha^4 g^2}\right)^{\frac{1}{4}} \tag{6.7}$$

is small. For the conditions of figure 6(*b*) this dimensionless group has the value 0.7, showing that for Provis's experiments viscosity near the island was not negligible (cf. the differences between figures 2(*a*) and 2(*b*)).

For edge-wave resonances the combination of terms $\omega^2 a/\alpha g$ is of order unity. Thus for experiments of different size the dimensionless group (6.7), with ω eliminated, scales as $\nu^{\frac{1}{4}}a^{-\frac{3}{8}}\alpha^{-\frac{5}{8}}g^{-\frac{1}{4}}$. Hence it is advantageous to increase both the island radius and the steepness of the beach. In the laboratory realistie beach slopes, of order 0.01, are therefore quite out of the question. In Provis's experiments even a slope of 0.1 was too modest to satisfy this requirement, yet a steeper slope would be inappropriate for the 'mild-slope' or 'longwave' approximations.

For the standing waves between the island and the wavemaker, the condition for negligible effects is that the wavemaker distance w is so large that the Hankel-function coefficients $H_n(2k_\infty w)$ in (4.7) are negligible. Alas, the decay rate is only

$$|H_n(2k_\infty w)| \sim [\pi k_\infty w]^{-\frac{1}{2}}. \tag{6.8}$$

Thus to get the errors down to 10% it would be necessary to have the wavemaker at least 5 wavelengths distant from the island. Even this modest level of accuracy would require a doubling of the size of Provis's wave basin (see figure 1).

Fortunately, Pite (1977) found a simple means of avoiding the troubles associated with the standing waves. He used a section of wave absorber (a bed of glass marbles) between the wavemaker and the island shelf. Any reflected waves from the island (see figure 3) would suffer double attenuation before returning to the island.

7. Conclusion

The reasonable agreement between the theoretical predictions shown in figure 6(*b*) and the experimental results shown in figure 7 gives us confidence in the theoretical modelling of waves over bottom topography of mild slope. However, instead of being dominated by the trapping of edge waves, Provis's (1975, 1976) experiments are strongly effected by viscous damping near the water line and by standing water between the island and the wavemaker.

Alas, the shortcomings of Provis's experiments are not due to lack of technique, but instead are due to intrinsic scaling difficulties. In wave experiments with gently sloping beaches, the effects of the reduced depth and increased wave amplitude compound to make viscosity much more important than in experiments with vertical boundaries. This can be ameliorated if steep beaches or large islands (longer waves) are used. Unless a wave absorber is used to suppress reflections between the wavemaker and the island (Pite 1977), there can be strong standing waves. At least five deep-water wavelengths are needed between the island shelf and the wavemaker.

This requirement, coupled with the desirability of large islands, puts great demands upon the size of the wave basin – demands which are way beyond the size of the laboratory that was available to Provis.

The authors wish to thank Dr David Provis for permission to reproduce his experimental results. R.S. was supported by the Royal Society and by British Petroleum.

Appendix. The dispersion relation for damped water waves

For a viscous fluid the mass conservation and linearized momentum equations for two-dimensional flow are

$$\frac{\partial u}{\partial x}+\frac{\partial w}{\partial z}=0, \quad \frac{\partial u}{\partial t}=-\frac{1}{\rho}\frac{\partial p}{\partial x}+\nu\nabla^2 u, \quad \frac{\partial w}{\partial t}=-\frac{1}{\rho}\frac{\partial p}{\partial z}+\nu\nabla^2 w. \quad \text{(A 1}a,b,c\text{)}$$

At the lower rigid boundary both components of velocity vanish:

$$u=0, \quad w=0 \quad (z=-h). \qquad \text{(A 2}a,b\text{)}$$

For small-amplitude motions the free-surface displacement ζ is related to the vertical velocity w by the kinematic boundary condition

$$\frac{\mathrm{d}\zeta}{\mathrm{d}t}=w \quad (z=0), \qquad \text{(A 3)}$$

and the normal stress must balance the sum of surface tension and the hydrostatic pressure:

$$-\frac{p}{\rho}+2\nu\frac{\partial w}{\partial z}=-g\zeta+T\frac{\partial^2\zeta}{\partial x^2} \quad (z=0). \qquad \text{(A 4)}$$

In general the shear stress at the surface is balanced by surface elastic forces. For simplicity we consider the extreme case of a dirty surface unable to move:

$$u=0 \quad (z=0). \qquad \text{(A 5)}$$

To solve the field equations (A 1) subject to the boundary conditions (A 2–5), we follow the procedure given by Lamb (1932, §349). The velocity field is decomposed into rotational and irrotational parts:

$$u=-\frac{\partial\psi}{\partial z}-\frac{\partial\phi}{\partial x}, \quad w=\frac{\partial\psi}{\partial x}-\frac{\partial\phi}{\partial z}. \qquad \text{(A 6}a,b\text{)}$$

This satisfies the mass-conservation and momentum equations (A 1a–c) provided that

$$\nabla^2\phi=0, \quad \nu\nabla^2\psi=\frac{\partial\psi}{\partial t}, \quad \frac{p}{\rho}=\frac{\partial\phi}{\partial t}. \qquad \text{(A 7}a,b,c\text{)}$$

In terms of ϕ and ψ the kinematic and normal-stress boundary conditions (A 3), (A 4) at the free surface can be combined:

$$\frac{\partial^2\phi}{\partial t^2}+2\nu\frac{\partial^2}{\partial t\,\partial z}\left(\frac{\partial\phi}{\partial z}-\frac{\partial\psi}{\partial x}\right)+\left(g-T\frac{\partial^2}{\partial x^2}\right)\left(\frac{\partial\phi}{\partial z}-\frac{\partial\psi}{\partial x}\right)=0 \quad (z=0). \qquad \text{(A 8)}$$

We now restrict attention to solutions with horizontal and temporal dependence $\exp(\mathrm{i}kx+\mathrm{i}\omega t)$. Appropriate representations for the z-dependence of the velocity potential ϕ and stream function ψ are

$$\hat{\phi} = A\cosh[k(z+h)]+B\sinh[k(z+h)], \tag{A 9a}$$

$$\hat{\psi} = C\cosh[m(z+h)]+D\sinh[m(z+h)], \tag{A 9b}$$

with

$$m^2 = \mathrm{i}\omega/\nu+k^2, \tag{A 9c}$$

where A, B, C, D are undetermined constants. The no-slip bottom boundary conditions require

$$\mathrm{i}kA+mD = 0, \quad -kB+\mathrm{i}C = 0. \tag{A 10}$$

Whence we can eliminate B, D:

$$\hat{\psi} = -\mathrm{i}B\cosh[m(z+h)]-\frac{\mathrm{i}k}{m}A\sinh[m(z+h)]. \tag{A 11}$$

The dirty-surface condition requires

$$Ak(\cosh kh-\cosh mh)+B(k\sinh kh-m\sinh mh) = 0, \tag{A 12}$$

and the combined boundary condition (A 8) yields

$$A\left\{-\omega^2\cosh kh+2\mathrm{i}\omega\nu k^2(\cosh kh-\cosh mh)+(gk+Tk^3)\left(\sinh kh-\frac{k}{m}\sinh mh\right)\right\}$$
$$+B\{-\omega^2\sinh kh+2\mathrm{i}\omega\nu k(k\sinh kh-m\sinh mh)+(gk+Tk^3)(\cosh kh-\cosh mh)\} = 0. \tag{A 13}$$

We can eliminate A and B from the above two equations, leaving the dispersion relation

$$\omega^2\left\{1-\frac{k\tanh kh}{m\tanh mh}\right\} = (gk+Tk^3)\tanh kh\left\{1-2\frac{k\coth kh}{m\tanh mh}+\left(\frac{k}{m}\right)^2+\frac{2k\,\mathrm{cosech}\,kh}{m\sinh mh}\right\}, \tag{A 14a}$$

with

$$m^2 = \mathrm{i}\omega/\nu+k^2. \tag{A 14b}$$

As we should expect, for small viscosity (i.e. for large m) this dispersion relation yields the well-known inviscid water-waves result

$$\omega^2 = (gk+Tk^3)\tanh kh. \tag{A 15}$$

REFERENCES

Abramowitz, M. & Stegun, I. A. 1964 *Handbook of Mathematical Functions.* Natl Bur. Standards Appl. Math. Ser.

Berkhoff, J. C. W. 1973 Computation of combined refraction–diffraction. In *Proc. 13th Coastal Engng Conf.* vol. 1, pp. 471–490.

Berkhoff, J. C. W. 1976 Mathematical models for simple harmonic linear water waves: wave diffraction and refraction. *Delft Hydraulic Lab. Rep.* no. 163.

Jonsson, I. G. & Brink-Kjaer, O. 1973 A comparison between two reduced wave equations for gradually varying depth. *Prog. Rep. Inst. Hydrodyn. Hydraul. Engng, Tech. Univ. Denmark* **31**, 13–18.

Jonsson, I. G. & Skovgaard, O. 1979 A mild-slope equation and its application to tsunami calculations. *Marine Geodesy* **2**, 41–58.

Lamb, H. 1932 *Hydrodynamics.* Cambridge University Press.

Longuet-Higgins, M. S. 1967 On the trapping of wave energy round islands. *J. Fluid Mech.* **29**, 781–821.

MAHONY, J. J. 1971 Excitation of surface waves near to a cut-off frequency. *Fluid Mech. Res. Inst. Rep. Univ. Essex* no. 7.

PITE, H. D. 1977 The excitation of damped waves diffracted over a submerged circular sill. *J. Fluid Mech.* **82**, 621–641.

PROVIS, D. G. 1975 Propagation of water waves near an island. Ph.D. thesis, University of Essex.

PROVIS, D. G. 1976 Experimental studies of wave refraction. In *Waves on Water of Variable Depth* (ed. D. G. Provis & R. Radok). Lecture Notes in Physics vol. 64, pp. 39–45. Springer.

SHEN, M. C. & KELLER, J. B. 1975 Uniform ray theory of surface, internal and acoustic wave propagation in a rotating ocean or atmosphere. *SIAM J. Appl. Maths* **28**, 857–875.

SHEN, M. C., MEYER, R. E. & KELLER, J. B. 1968 Spectra of water waves in channels and around islands. *Phys. Fluids* **11**, 2289–2304.

SMITH, R. 1974 Edge waves on a beach of mild slope. *Q. J. Mech. Appl. Maths* **27**, 102–110.

SMITH, R. 1975 Second-order turning point problems in oceanography. *Deep-Sea Res.* **22**, 837–852.

SMITH, R. & SPRINKS, T. 1975 Scattering of surface waves by a conical island. *J. Fluid Mech.* **72**, 373–384.